Thin Solid Films 645 (2018) 417–423

Contents lists available at ScienceDirect

Thin Solid Films

journal homepage: www.elsevier.com/locate/tsf

Hydrothermally grown ZnO electrodes for improved organic photovoltaic devices

P. Steiger[a,1], J. Zhang[a], K. Harrabi[b], I.A. Hussein[c], J.M. Downing[a], M.A. McLachlan[a,*]

[a] Department of Materials & Centre for Plastic Electronics, Imperial College London, SW7 2AZ, UK
[b] Physics Department & Center of Research Excellence in Renewable Energy (CoRERE), Research Institute, King Fahd University of Petroleum & Minerals, Dhahran 31261, Saudi Arabia
[c] Gas Processing Centre, Qatar University, Doha, Qatar

ABSTRACT

Here we report a simple, solution based processing route for the formation of large surface area electrodes resulting in improved organic photovoltaic devices when compared with conventional planar electrodes. The nanostructured electrode arrays are formed using hydrothermally grown ZnO nanorods, subsequently infiltrated with blends of poly(3-hexylthiophene-2,5-diyl) (P3HT) and indene-C_{60} bisadduct ($IC_{60}BA$) as photoactive materials. This well studied organic photoactive blend allows the composition/processing/performance relationships to be elucidated. Using simple solution based processing the resultant nanostructured devices exhibited a maximum power conversion efficiency (PCE) of 2.5% compared with the best planar analogues having a PCE of around 1%. We provide detailed structural, optical and electrical characterization of the nanorod arrays, active layers and completed devices giving an insight into the influence of composition and processing on performance. Devices were fabricated in the desirable inverse geometry, allowing oxidation resistant high work-function top electrodes to be used and importantly to support the hydrothermal growth of nanorods on the bottom electrode — all processing was carried out under ambient conditions and without the insertion of a hole transport layer below the anode. The nanorods were successfully filled with the active layer materials by carrying out a brief melt processing of a spin-cast top layer followed by a subsequent thermal anneal which was identified as an essential step for the fabrication of operational devices. The growth method used for nanorod fabrication and the active layer processing are both inherently scalable, thus we present a complete and facile route for the formation of nanostructured electron acceptor layers that are suitable for *high performance* organic active layers.

1. Introduction

Organic photovoltaics (OPVs) are now routinely reported with power conversion efficiencies (PCEs) exceeding 10% [1–3], with recent devices showing continued improvements in PCE to report values above 13% in devices combining polymer absorbers with non-fullerene acceptor species [4]. This rapid acceleration of performance has been enabled through a combination of advances in synthesis and the development of new active layer materials, improvements in charge transport and through a greater understanding of the required device morphology and microstructure. Significantly, increased photogenerated charge within an active layer only contributes to the measured photocurrent of a device if the charge carriers can be collected. The incorporation of metal oxide charge extraction layers in OPV devices has been demonstrated as a feasible method for improving device performance by simultaneously improving charge extraction and by allowing the preparation of more stable inverted devices [5]. ZnO in particular has been utilized as a hole blocking, electron transport layer [6,7]. ZnO is an excellent candidate material for compatibility for OPVs owing to its excellent electronic properties and suitability for low-temperature processing *via* solution or physical deposition methods [8,9]. ZnO has similar electronic properties to TiO_2 [10] but has greater electron mobility and has the advantage that tunable electronic and morphological properties can be readily obtained through modifications in the preparation method [11]. It has been proposed that oriented nanostructures, such as nanorods, can provide significantly larger interfacial areas for charge collection in addition to providing a direct pathway for electron transport where the absence of grain boundaries in the single crystal rods increases charge carrier mobilities [12,13]. Moreover, the ordered structures provide a straight *i.e.* vertical

* Corresponding author.
E-mail address: martyn.mclachlan@imperial.ac.uk (M.A. McLachlan).
[1] Now at Paul Scherrer Institut, OSUA/101, 5232 Villigen PSI, Switzerland.

https://doi.org/10.1016/j.tsf.2017.11.021
Received 11 January 2016; Received in revised form 10 November 2017; Accepted 14 November 2017
Available online 15 November 2017
0040-6090/

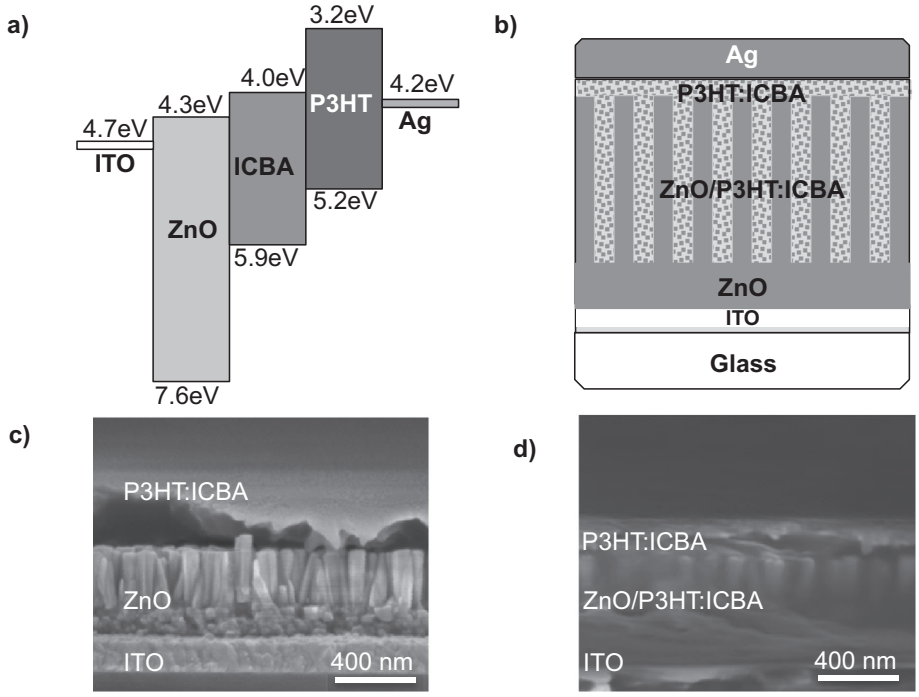

Fig. 1. Schematic illustrations showing a) device structure and flat-band energy level diagram for the devices investigated [38], b) idealized diagram of NRA device architecture, c) SEM micrograph showing NRA with spin cast over layer of active materials, d) SEM micrograph showing typical device structure following melt processing and thermal anneal.

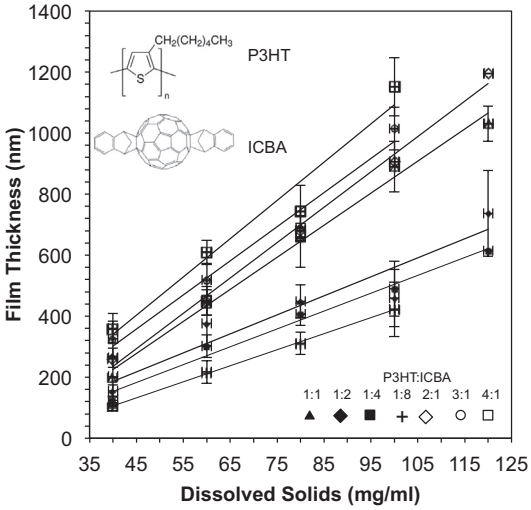

Fig. 2. Plot showing the variation in film thickness for a range of P3HT: $IC_{60}BA$ ratios and solution concentrations. Films spin-cast from chlorobenzene with thicknesses measured using surface profilometry.

channel for filling with the active material or, in the case of dye sensitized cells, the electrolyte [14,15]. The preparation of ordered 2D nanorods has been well reported using the hydrothermal method [16], which allows the large area deposition of controlled aspect ratio nanorods with a high degree of vertical alignment [17]. The short exciton diffusion lengths (~10 nm) and the comparably low charge carrier mobilities in organic semiconducting materials require that the acceptor and donor components of the active layer be dispersed by no more than around 10 nm. It is further required that both networks (acceptor and donor) are continuous in order to allow for efficient electron and hole transportation to the electrodes over distances of a few hundred nanometers [18]. Thus the incorporation of nanostructured oxide arrays – such as nanorods – provides a convenient method of enhancing charge collection. While strategies to prepare hybrid photovoltaics *i.e.* where the oxide acts as both an active material *and* the electron transport layer have had limited success [19–22] the incorporation of a nanostructured electron acceptor here, using simple device structures processed in ambient, is shown to improve performance. Unlike previous reports where multistep patterning was required or where non-standard conjugated materials utilized [23] here we describe the preparation of bulk heterojunction photovoltaic devices using the commonly used, widely available active materials poly(3-hexylthiophene-2,5-diyl) (P3HT) — indene-C_{60} bisadduct ($IC_{60}BA$) using planar and nanostructured ZnO electron extracting layers and report on the device improvements enabled by incorporating nanorod electrodes and the impact these electrodes have on the optimum active layer composition.

2. Experimental details

All devices were prepared using pre-patterned indium tin oxide (ITO) substrates (Psiotec UK Ltd., 12–16 Ω/square) washed sequentially with the aid of ultrasonics using OptiClear, acetone, isopropanol and deionized water before a final N_2 dry. A 10-minute UV/ozone exposure was implemented as the final cleaning step before use.

The nanorod (NR) deposition method has been previously reported in detail [17,24], this briefly consists of two stages i) deposition of a dense ZnO planar layer and, ii) subsequent hydrothermal growth of the NR array. Here the planar layer was cast by spin coating from a sol-gel consisting of equal concentrations of zinc acetate dihydrate and 2-aminoethanol made up to 0.75 mol dm^{-3} in 2-methoxyethanol. Once cast, the substrates were annealed for 10 min at 300 °C, before another coating was applied. This step was repeated three times. Finally the substrates were annealed for 60 min at 450 °C to aid the densification and improve crystallinity, with final thickness of approximately 130 nm. Nanorod synthesis was achieved by suspending the substrates in an aqueous bath containing equimolar (50 mmol dm^{-3}) zinc nitrate hexahydrate $[Zn(NO_3)_2{\cdot}6H_2O]$ and hexamethylenetetramine $[NH_2(CH_2)_6NH(CH_2)_6NH_2]$, in addition to 200 mmol dm^{-3} KCl and 20 mmol dm^{-3} polyethylenimine $[H(NHCH_2CH_2)_nNH_2]$. The reaction was allowed to proceed until 500 nm rods were formed. In summary, highly crystalline, (002) orientated, transparent NR films are prepared in all cases with calculated band gaps in the range of 3.2–3.3 eV.

Solutions of P3HT [25] (M_w ~ 85 kg mol^{-1}), $IC_{60}BA$ (Ossila UK Ltd.) and blends thereof were prepared using chlorobenzene as the

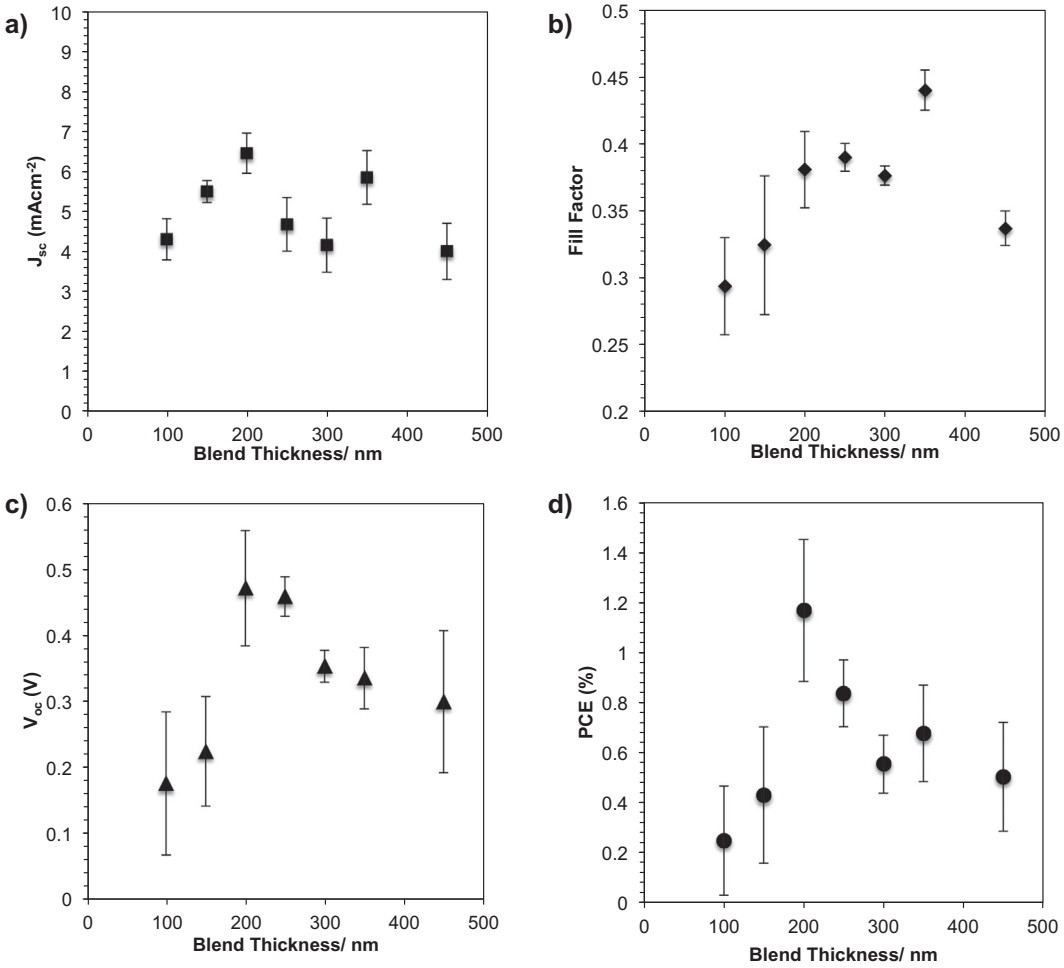

Fig. 3. a–d) Measured performance characteristics for devices prepared using a planar ZnO active layer with a 1:1 P3HT: $IC_{60}BA$ active layer of variable thickness, e) representative current density-voltage (J-V) plots for various active layer thicknesses).

solvent. After solvent addition the glass flasks were wrapped in aluminum foil to exclude light and the solutions were stirred on a magnetic stirrer overnight (16 h) in a dry glovebox under nitrogen atmosphere. Prior to deposition, the solutions were heated to 90 °C on a hotplate. Homogeneous thin films on clean glass substrates were obtained by spin-coating using a two-step procedure: 2 s at 500 rpm then 60 s at 2000 rpm. Devices were completed by thermal evaporation of Ag electrodes through a shadow mask to produce of ~140 nm thick electrodes. For the preparation of nanorod devices a multistep polymer deposition process was here developed and employed throughout. Firstly, the blend solution was spin-cast directly onto the nanorods as detailed above. The blend solution typically capped the nanorods and little infiltration resulted after spin-coating. Next, the nanorod/active layer was heated to 240 °C for 3 min, which resulted in the active layer completely filling the nanorod arrays. A final anneal at 150 °C was carried out for various time periods as described in the main text.

Film thicknesses were measured at five locations using well-defined scratches using a surface profilometer (Veeco, Dektak 150). Scanning electron microscopy (SEM) characterization of nanorod arrays and completed devices were obtained using a LEO 1525 field emission instrument operated at 2–10 kV. When necessary, a thin (15 nm) layer of Cr was deposited on the samples to minimize charging effects. Devices were tested on a Newport Oriel Solar Simulator using a xenon arc lamp filtered to AM 1.5 operating at 100 mW cm^{-2}. Current density-voltage (J-V) curves were obtained from 1.0 V to − 1.0 V (Keithley 2420 Source Meter) from which the open circuit voltage (V_{OC}), short circuit current density (J_{SC}), the fill factor (FF) and power conversion efficiency (PCE) were calculated.

3. Results & discussion

The flat-band energy level diagram for the devices prepared is shown in Fig. 1a, also shown is a schematic illustration of the nanorod devices (Fig. 1b). To determine the relationship between active layer composition and thickness planar films were initially cast on glass substrates using a wide range of dissolved solid concentrations (40–120 mg/ml) and P3HT:$IC_{60}BA$ weight ratios (1:4 to 4:1) (Fig. 2). Linear profilometry measurements showed no observable aggregates after film formation, confirming our conditions lie within the solubility limits of the organic materials investigated [26]. As anticipated there is a steady increase in film thickness as the dissolved solid concentration increases. In parallel, significant variations in thickness are also observed as the composition is varied, with the polymer rich films being significantly thicker than their fullerene rich analogues. The information obtained from this thickness/composition analysis allowed thick films to be cast on nanorod substrate in a single deposition step.

As a benchmark to the performance of bulk heterojunction devices, planar ZnO *i.e.* a non-nanostructured electron transport layer was used first investigated. Using a P3HT:$IC_{60}BA$ blend ratio of 1:1 [27] the active layer thickness was varied from 100 to 450 nm, for these devices a post deposition anneal at 150 °C was carried out for 10 min. Representative device characteristics are shown in Fig. 3, where the highest PCEs are obtained for 200 nm thick active layers. In general the V_{OC}, J_{SC} and FF for these devices are lower than previous reports for

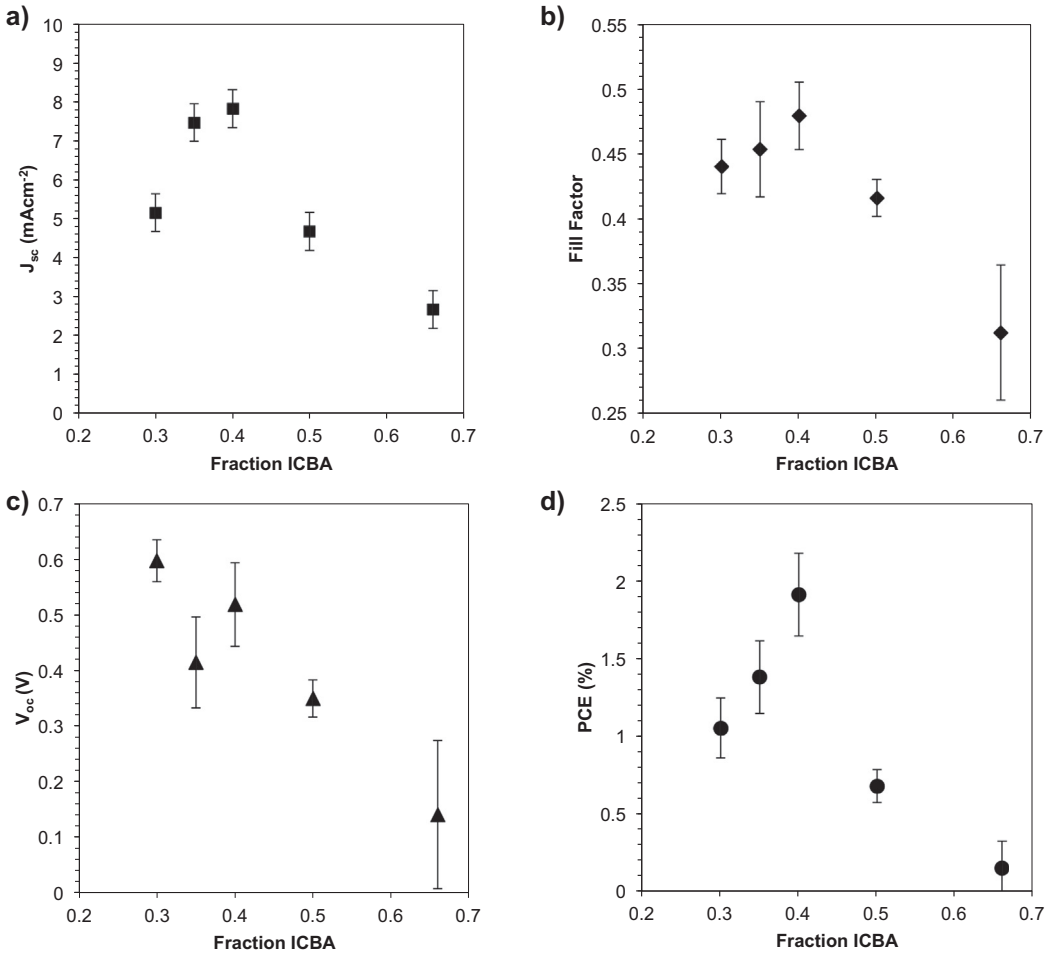

Fig. 4. a–d) Measured performance characteristics for devices prepared using nanostructured ZnO electrodes with various P3HT: $IC_{60}BA$ ratios, the best performing composition is determined to be 3:2, e) representative current density-voltage (J-V) plots for several active layer compositions.

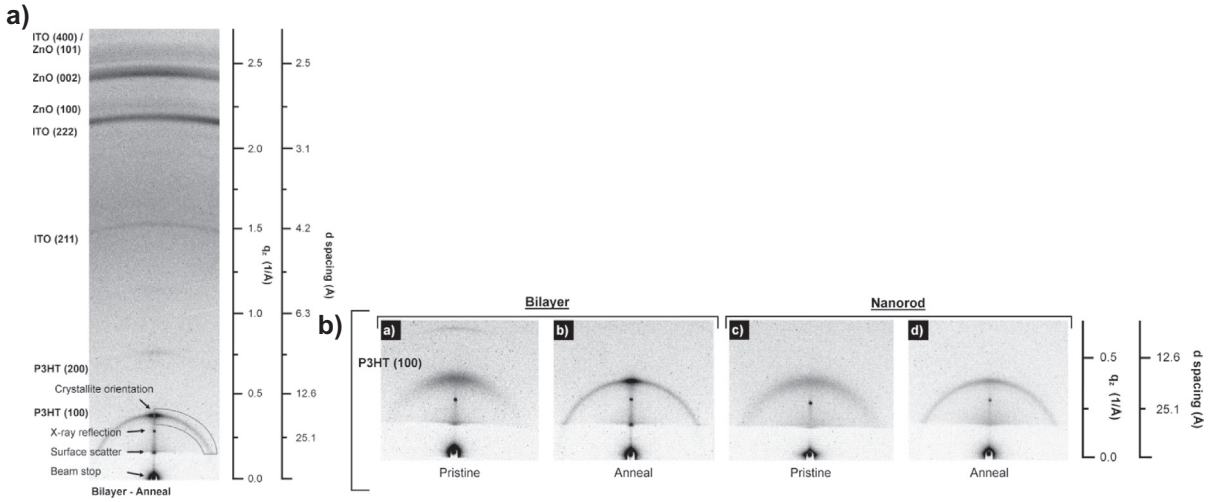

Fig. 5. a) SAXS pattern for P3HT (30 K) on planar ZnO, showing characteristic scattering arcs for ZnO:P3HT samples. Labeled on the pattern are points of high scattering intensity resulting from direct transmission, surface and reflection from the surface and P3HT crystallite orientation perpendicular to the substrate. The box overlaid on the pattern shows the boundaries of an integration for quantifying crystallite orientation from the P3HT (100) plane, b) SAXS patterns for P3HT (a–d) for polymer films on planar sol-gel ZnO and ZnO nanorod substrates. Films were examined after spin coating with no further treatment (pristine) or after a slow heating and cooling program (anneal) as described in the main text.

this composition [27,28], this may be attributed to the absence of an electron-blocking layer at the cathode which would not however influence the overall trends observed.

Based on our previous work we chose to utilize 500 nm nanorods grown onto the planar seed layers as nanostructured electrodes [29]. An equivalent active layer thickness of 250 nm was identified as sufficient to infiltrate the arrays and prevent short-circuiting (Fig. 1c–d). For efficient device performance, the active layer must penetrate the entire volume of the oxide array, which is difficult to achieve for a densely packed structure with a very large surface area [26]. To overcome this

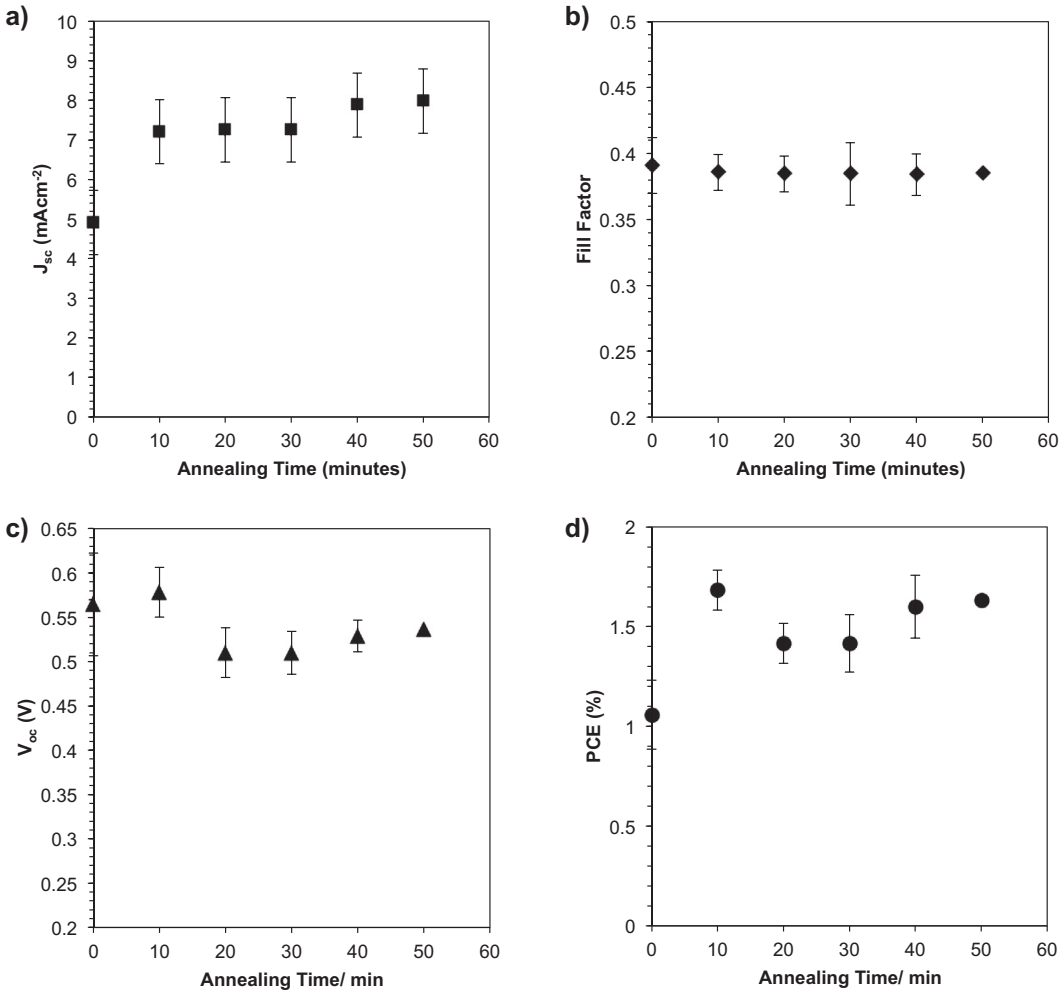

Fig. 6. a–d) Device characteristics for nanorod/P3HT: $IC_{60}BA$ (3:2) devices showing the influence of 150 °C anneal on performance, improvements are only observed with a 10-minute anneal.

Table 1
Measured nanorod device characteristics highlighting the impact of post deposition anneal (150 °C for 10 min) for 12 device pixels (brackets give standard deviations).

	PCE (%)	J_{SC} (mA cm^{-2})	V_{OC} (V)	FF
No anneal	0.04 (0.02)	1.47 (0.26)	0.09 (0.06)	0.30 (0.03)
Annealed	1.21 (0.13)	5.81 (0.31)	0.49 (0.06)	0.43 (0.04)

challenge we have developed a 2-step filling methodology that affords the use of standard, commercially available photoactive materials, where firstly the nanorods are coated with a thick active layer blend that is then melt processed into the nanorod arrays and subsequently annealed at 150 °C [14]. When the filling was optimized we studied the influence of the active layer composition. The previously reported P3HT:$IC_{60}BA$ ratio of 1:1 was varied between 3:1 and 1:2 and the device characteristics assessed (Fig. 4). It is apparent that the optimum J_{SC}, FF and PCE are obtained at a P3HT: $IC_{60}BA$ of 3:2 *i.e.* a polymer rich composition. The origin of this deviation may relate to the thermally induced phase segregation and vertical separation of the active layer, creating a P3HT rich region close to the ZnO occupying a larger surface area than non-nanostructured devices [30]. At high $IC_{60}BA$ ratios *i.e.* above 1:1, measured J_{SC} values are reduced due to the lack of spectral overlap between $IC_{60}BA$ in the 300–400 nm region and the incident illumination.

The fundamental V_{OC} value is determined by the offset between the lowest unoccupied molecular orbital (LUMO) level of the fullerene and the highest occupied molecular energy (HOMO) level of P3HT, in addition to contributions from the electronic band gap, charge carrier density and slope and density in gap states of the bulk heterojunction [31]. Variation of $IC_{60}BA$ concentration in such films not only affects the molecular morphology, by changing the ability for polymer chains to crystallize, but also the electronic structure of the films. Here, as noted previously, at high $IC_{60}BA$ concentrations the net optical absorption is reduced and V_{OC} reduces correspondingly due to reduction in charge carrier density and position of these charges within the device. We speculate that the observed V_{OC} reduction with increasing $IC_{60}BA$ fraction is attributed to penetration of $IC_{60}BA$ into crystalline P3HT domains thus impacting the energy levels of acceptor and donor phases. This intermixing of the two components may not only affect the charge mobility [32] but also the position of the acceptor and donor energy levels which then in turn influences V_{OC}.

P3HT is known to form self-organized structures upon annealing [33]. Regular stacking of the individual P3HT chains is beneficial for charge transport as it increases the charge mobility in the direction of stacking through intermolecular π-π interactions and it also benefits absorption at longer wavelengths as inter-chain interactions are enhanced [34]. The nucleation and growth and therefore the size of these self-organized P3HT domains can be controlled by appropriate annealing conditions which allows for tuning and optimizing of the bulk heterojunction morphology and subsequent device performance increase [35]. Small angle X-ray scattering (SAXS) was used to investigate the orientation of P3HT on planar ZnO substrates and also in ZnO

nanorod arrays. A typical SAXS pattern for P3HT on planar ZnO is labeled clearly in Fig. 5a. In Fig. 5b the complete SAXS data set for the scattering arc from the P3HT (100) plane are shown. For pristine polymer films on planar substrates the P3HT arc is diffuse with the majority of scattering in the out-of-plane [100] direction. After annealing the arc becomes narrower; indicating increased uniformity in the distance between polymer chains, due to improvements in polymer crystallinity. The intensity is at a maximum perpendicular to the substrate, showing that the majority of crystallite (100) planes are orientated in this direction. While this is the preferred orientation for P3HT [36], it is also worth noting that intensity at all points along the arc are increased, showing that many crystallites have an orientation between the vertical and horizontal *i.e.* mixed orientation. Although there is an increase in crystallinity (as seen from the reduced arc width in Fig. 5d), there is little change in the orientation between pristine and annealed samples. In contrast P3HT on ZnO planar layers are seen to orientate with a strong in-plane character. Nanorod arrays provide a template for this orientation in 2-D allowing for both in-plane orientation to the seed layer and in plane orientation to the nanorod walls. This may result in the observed higher degree of mixed orientation in nanorod samples.

To further probe the influence of annealing in our nanostructured arrays a series of devices were prepared using the optimized 3:2 P3HT:$IC_{60}BA$ ratio and annealed at 150 °C for various time periods. The results obtained, Fig. 6, show an improvement in PCE, attributed to the improvements in J_{SC} during the initial 10-min anneal. Extending the annealing time, up to 50 min, has little overall effect on the device performance with no systematic changes observed. After melt infiltration the blend is rapidly quenched thus the active layer composition will likely less crystalline, thermal annealing is necessary to induce crystallization of the P3HT and aggregation of the $IC_{60}BA$. The high aspect ratio channels formed in the nanorod arrays may mean that the optimum active layer microstructure can be achieved rapidly [37] as these channels are typically laterally separated by < 50 nm compared with the active layer thickness of ~500 nm. To emphasize the importance of controlling the composition of the active layer in addition to the post deposition annealing we highlight the remarkable changes in performance noted for the non-optimized 1:1 blend composition, Table 1, using comparable device structures to those shown in Fig. 1c–d. Performance enhancements attributed to thermal annealing in planar devices have been reported in detail by Kippelen et al. In our case penetration of nanorods into the active layer and their surface energies may induce segregation of P3HT to the vertical *and* horizontal oxide interfaces, which results in the optimum photoactive layer composition for our non-planar devices.

4. Conclusions

Here we have demonstrated the effective implementation of nanostructured ZnO cathodes into organic bulk heterojunction photovoltaic devices using a solution-processing route for electrode fabrication followed by a simple infiltration process using commercially available materials. In comparison with planar analogues we observe a significant improvement in measured device performance, attributed to the increased surface area of electron accepting material. We highlight the importance of thermal annealing of the active layer to obtain optimal active layer morphologies. Additionally, we have seen a deviation from the composition of the active layer compared with planar devices, attributed to the ZnO acting as a junction for exciton separation thus reducing the quantity of fullerene required. The increased content of P3HT in our nanostructured devices is likely to contribute to the observed improvements owing to greater absorption over the 450–650 nm range resulting in increased photogeneration compared with planar devices. While previous reports have highlighted the limitations of oxide:polymer active layers here we have shown that solution processed oxide nanostructures can be readily and controllably prepared and effectively implemented in improved photovoltaic devices.

Acknowledgments

J.D. was supported through an EPRSC project EP/J016039/1, J.Z. as a PhD through the China Scholarship Council. K.H., I.A.H. and M.A.M. thank the National Plan for Science, Technology and Innovation (MAARIFAH) – King Abdulaziz City for Science and Technology – for funding through the Science & Technology Unit at King Fahd University of Petroleum & Minerals (KFUPM) – the Kingdom of Saudi Arabia, award number 12-ENE2379-04. All authors gratefully acknowledge Prof. John de Mello and Dr. James Bannock (Imperial) for providing the P3HT used in this study. A portion of this research (SAXS) was conducted at the Center for Nanophase Materials Sciences, which is a DOE Office of Science User Facility – we are extremely grateful to Dr. Andrew Payzant for supporting the SAXS measurements and assisting with data interpretation.

References

[1] Research Cell Efficiency Records, Natl. Renew. Energy Lab. (2017). https://www.nrel.gov/pv/assets/images/efficiency-chart.png.
[2] M.A. Green, K. Emery, Y. Hishikawa, W. Warta, E.D. Dunlop, Solar cell efficiency tables (version 48), Prog. Photovolt. Res. Appl. 24 (2016) 905–913, http://dx.doi.org/10.1002/pip.2788.
[3] A.A.L.K. Jagadamma, M. Al-Senani, A. El-Labban, I. Gereige, G.O. Ngongang Ndjawa, J.C.D. Faria, T. Kim, K. Zhao, F. Cruciani, D.H. Anjum, M.A. McLachlan, P.M. Beaujuge, Polymer solar cells with efficiency > 10% enabled via a facile solution-processed Al-doped ZnO electron transporting layer, Adv. Energy Mater. 5 (2015) 1500204, http://dx.doi.org/10.1002/aenm.201500204.
[4] W. Zhao, S. Li, H. Yao, S. Zhang, Y. Zhang, B. Yang, J. Hou, Molecular optimization enables over 13% efficiency in organic solar cells, J. Am. Chem. Soc. (2017), http://dx.doi.org/10.1021/jacs.7b02677.
[5] S. Schumann, D. Campo, B. Illy, A.C. Cruickshank, M.A. McLachlan, M.P. Ryan, D.J. Riley, D.W. McComb, T.S. Jones, Inverted organic photovoltaic devices with high efficiency and stability based on metal oxide charge extraction layers, J. Mater. Chem. 21 (2011) 2381–2386, http://dx.doi.org/10.1039/C0JM03048A.
[6] M.T. Lloyd, D.C. Olson, P. Lu, E. Fang, D.L. Moore, M.S. White, M.O. Reese, D.S. Ginley, J.W.P. Hsu, Impact of contact evolution on the shelf life of organic solar cells, J. Mater. Chem. 19 (2009) 7638, http://dx.doi.org/10.1039/b910213b.
[7] B. Gholamkhass, N.M. Kiasari, P. Servati, An efficient inverted organic solar cell with improved ZnO and gold contact layers, Org. Electron. 13 (2012) 945–953, http://dx.doi.org/10.1016/j.orgel.2012.02.012.
[8] Y.H. Lin, H. Faber, K. Zhao, Q. Wang, A. Amassian, M.A. McLachlan, T.D. Anthopoulos, Y.-H. Liu, H. Faber, K. Zhao, Q. Wang, A. Amassian, M.A. McLachlan, T.D. Anthopoulos, High-performance ZnO transistors processed via an aqueous carbon-free metal oxide precursor route at temperatures between 80–180 °C, Adv. Mater. 25 (2013) 4340–4346, http://dx.doi.org/10.1002/adma.201301622.
[9] J.B. Franklin, B. Zou, P. Petrov, D.W. McComb, M.P. Ryan, M.A. McLachlan, J.B. Franklin, B. Zou, D.W. McComb, P. Petrov, M.P. Ryan, M.A. McLachlan, Optimised pulsed laser deposition of ZnO thin films on transparent conducting substrates, J. Mater. Chem. 21 (2011) 8178–8182, http://dx.doi.org/10.1039/c1jm10658a.
[10] S. Gärtner, M. Christmann, S. Sankaran, H. Röhm, E.-M. Prinz, F. Penth, A. Pütz, A.E. Türeli, B. Penth, B. Baumstümmler, A. Colsmann, Eco-friendly fabrication of 4% efficient organic solar cells from surfactant-free P3HT:ICBA nanoparticle dispersions, Adv. Mater. 26 (2014) 6653–6657, http://dx.doi.org/10.1002/adma.201402360.
[11] Z.L. Wang, Nanostructures of zinc oxide, Mater. Today 7 (2004) 26–33, http://dx.doi.org/10.1016/S1369-7021(04)00286-X.
[12] J. Weickert, H.C. Hesse, W. Wiedemann, L. Schmidt-Mende, Nanostructured organic and hybrid solar cells, Adv. Mater. 23 (2011) 1810–1828, http://dx.doi.org/10.1002/adma.201003991.
[13] I. Gonzalez-Valls, M. Lira-Cantu, Vertically-aligned nanostructures of ZnO for excitonic solar cells: a review, Energy Environ. Sci. 2 (2009) 19–34, http://dx.doi.org/10.1039/B811536B.
[14] J.C.D. Faria, A.J. Campbell, M.A. McLachlan, ZnO nanorod arrays as electron injection layers for efficient organic light emitting diodes, Adv. Funct. Mater. 25 (2015) 4657–4663, http://dx.doi.org/10.1002/adfm.201501411.
[15] S. Yun, J. Lee, J. Chung, S. Lim, Improvement of ZnO nanorod-based dye-sensitized solar cell efficiency by Al-doping, J. Phys. Chem. Solids 71 (2010) 1724–1731, http://dx.doi.org/10.1016/j.jpcs.2010.08.020.
[16] L. Vayssieres, Growth of arrayed nanorods and nanowires of ZnO from aqueous solutions, Adv. Mater. 15 (2003) 464–466, http://dx.doi.org/10.1002/adma.200390108.
[17] J.M. Downing, M.P. Ryan, M.A. McLachlan, Hydrothermal growth of ZnO nanorods: the role of KCl in controlling rod morphology, Thin Solid Films 539 (2013) 18–22, http://dx.doi.org/10.1016/j.tsf.2013.04.131.
[18] B.C. Thompson, J.M.J. Fréchet, Polymer–fullerene composite solar cells, Angew.

Chem. Int. Ed. 47 (2008) 58–77, http://dx.doi.org/10.1002/anie.200702506.
[19] L. Baeten, B. Conings, H.-G. Boyen, J. D'Haen, A. Hardy, M. D'Olieslaeger, J.V. Manca, M.K. Van Bael, L. Baeten, B. Conings, H.-G. Boyen, J. D'Haen, A. Hardy, M. D'Olieslaeger, J.V. Manca, M.K. Van Bael, Towards efficient hybrid solar cells based on fully polymer infiltrated ZnO nanorod arrays, Adv. Mater. 23 (2011) 2802–2805, http://dx.doi.org/10.1002/adma.201100414.
[20] Y.-J. Lee, M.T. Lloyd, D. Olson, R.K. Grubbs, P. Lu, R.J. Davis, J.A. Voigt, J.W.P. Hsu, Optimization of ZnO nanorod array morphology for hybrid photovoltaic devices, J. Phys. Chem. C 113 (2009) 15778–15782, http://dx.doi.org/10.1021/jp904387z.
[21] O. Pachoumi, A.A. Bakulin, A. Sadhanala, H. Sirringhaus, R.H. Friend, Y. Vaynzof, Improved performance of ZnO/polymer hybrid photovoltaic devices by combining metal oxide doping and interfacial modification, J. Phys. Chem. C 118 (2014) 18945–18950, http://dx.doi.org/10.1021/jp506266f.
[22] S. Obuchovsky, I. Deckman, M. Moshonov, T. Segal Peretz, G. Ankonina, T.J. Savenije, G.L. Frey, Atomic layer deposition of zinc oxide onto and into P3HT for hybrid photovoltaics, J. Mater. Chem. C 2 (2014) 8903–8910, http://dx.doi.org/10.1039/C4TC01629G.
[23] S. Kim, J.H. Koh, X. Yang, W.S. Chi, C. Park, J.W. Leem, B. Kim, S. Seo, Y. Kim, J.S. Yu, J.H. Kim, E. Kim, Enhanced device efficiency of bilayered inverted organic solar cells based on photocurable P3HTs with a light-harvesting ZnO nanorod array, Adv. Energy Mater. 4 (2014) 1301338, , http://dx.doi.org/10.1002/aenm.201301338.
[24] J. Downing, M.P. Ryan, N. Stingelin, M.A. McLachlan, Solution processed hybrid photovoltaics: preparation of a standard ZnO template, J. Photonics Energy 1 (2011), http://dx.doi.org/10.1117/1.3569104.
[25] J.H. Bannock, S.H. Krishnadasan, A.M. Nightingale, C.P. Yau, K. Khaw, D. Burkitt, J.J.M. Halls, M. Heeney, J.C. de Mello, Continuous synthesis of device-grade semiconducting polymers in droplet-based microreactors, Adv. Funct. Mater. 23 (2013) 2123–2129, http://dx.doi.org/10.1002/adfm.201203014.
[26] F. Machui, S. Langner, X. Zhu, S. Abbott, C.J. Brabec, Determination of the P3HT:PCBM solubility parameters via a binary solvent gradient method: impact of solubility on the photovoltaic performance, Sol. Energy Mater. Sol. Cells 100 (2012) 138–146, http://dx.doi.org/10.1016/j.solmat.2012.01.005.
[27] G. Zhao, Y. He, Y. Li, 6.5% efficiency of polymer solar cells based on poly(3-hexylthiophene) and indene-C(60) bisadduct by device optimization, Adv. Mater. 22 (2010) 4355–4358, http://dx.doi.org/10.1002/adma.201001339.
[28] F. Cheng, G. Fang, X. Fan, H. Huang, Q. Zheng, P. Qin, H. Lei, Y. Li, Enhancing the performance of P3HT:ICBA based polymer solar cells using LiF as electron collecting buffer layer and UV–ozone treated MoO_3 as hole collecting buffer layer, Sol. Energy Mater. Sol. Cells 110 (2013) 63–68, http://dx.doi.org/10.1016/j.solmat.2012.12.006.
[29] J.M. Downing, Control and Characterisation of Metal Oxide/Polymer Morphologies for Hybrid Photovoltaic Devices, PhD thesis Imperial College London, 2013.
[30] H. Cheun, J.D. Berrigan, Y. Zhou, M. Fenoll, J. Shim, C. Fuentes-Hernandez, K.H. Sandhage, B. Kippelen, Roles of thermally-induced vertical phase segregation and crystallization on the photovoltaic performance of bulk heterojunction inverted polymer solar cells, Energy Environ. Sci. 4 (2011) 3456, http://dx.doi.org/10.1039/c1ee01316e.
[31] L.C.C. Elliott, J.I. Basham, K.P. Pernstich, P.R. Shrestha, L.J. Richter, D.M. DeLongchamp, D.J. Gundlach, Probing charge recombination dynamics in organic photovoltaic devices under open-circuit conditions, Adv. Energy Mater. 4 (2014) 1400356, , http://dx.doi.org/10.1002/aenm.201400356.
[32] Y.-H. Lin, Y.-T. Tsai, C.-C. Wu, C.-H. Tsai, C.-H. Chiang, H.-F. Hsu, J.-J. Lee, C.-Y. Cheng, Comparative study of spectral and morphological properties of blends of P3HT with PCBM and ICBA, Org. Electron. 13 (2012) 2333–2341, http://dx.doi.org/10.1016/j.orgel.2012.07.023.
[33] F.P.V. Koch, J. Rivnay, S. Foster, C. Mueller, J.M. Downing, E. Buchaca-Domingo, P. Westacott, L. Yu, M. Yuan, M. Baklar, Z. Fei, C. Luscombe, M.A. McLachlan, M. Heeney, G. Rumbles, C. Silva, A. Salleo, J. Nelson, P. Smith, N. Stingelin, The impact of molecular weight on microstructure and charge transport in semicrystalline polymer semiconductors poly(3-hexylthiophene), a model study, Prog. Polym. Sci. 38 (2013) 1978–1989, http://dx.doi.org/10.1016/j.progpolymsci.2013.07.009.
[34] R. Österbacka, C.P. An, X.M. Jiang, Z.V. Vardeny, Two-dimensional electronic excitations in self-assembled conjugated polymer nanocrystals, Science 287 (2000), http://dx.doi.org/10.1126/science.287.5454.839.
[35] G. Li, V. Shrotriya, J. Huang, Y. Yao, T. Moriarty, K. Emery, Y. Yang, G. Li, V. Shrotriya, J. Huang, Y. Yao, T. Moriarty, K. Emery, Y. Yang, High-efficiency solution processable polymer photovoltaic cells by self-organization of polymer blends, Nat. Mater. 4 (2005) 864–868, http://dx.doi.org/10.1038/nmat1500.
[36] R.J. Kline, M.D. McGehee, Morphology and charge transport in conjugated polymers, J. Macromol. Sci. C Polym. Rev. J. 46 (2007) 27–45, http://dx.doi.org/10.1080/15321790500471194.
[37] N.D. Treat, M.A. Brady, G. Smith, M.F. Toney, E.J. Kramer, C.J. Hawker, M.L. Chabinyc, Interdiffusion of PCBM and P3HT reveals miscibility in a photovoltaically active blend, Adv. Energy Mater. 1 (2011) 82–89, http://dx.doi.org/10.1002/aenm.201000023.
[38] N. Li, T. Stubhan, N.A. Luechinger, S.C. Halim, G.J. Matt, T. Ameri, C.J. Brabec, Inverted structure organic photovoltaic devices employing a low temperature solution processed WO_3 anode buffer layer, Org. Electron. 13 (2012) 2479–2484, http://dx.doi.org/10.1016/j.orgel.2012.06.045.